Pediatric Radiology (2018) 48:941–953
https://doi.org/10.1007/s00247-018-4127-7

ORIGINAL ARTICLE

Free-breathing quantification of hepatic fat in healthy children and children with nonalcoholic fatty liver disease using a multi-echo 3-D stack-of-radial MRI technique

Tess Armstrong[1,2] · Karrie V. Ly[3] · Smruthi Murthy[3] · Shahnaz Ghahremani[1] · Grace Hyun J. Kim[1] · Kara L. Calkins[3] · Holden H. Wu[1,2]

Received: 17 November 2017 / Revised: 7 February 2018 / Accepted: 25 March 2018 / Published online: 4 May 2018

Abstract

Background In adults, noninvasive chemical shift encoded Cartesian magnetic resonance imaging (MRI) and single-voxel magnetic resonance (MR) spectroscopy (SVS) accurately quantify hepatic steatosis but require breath-holding. In children, especially young and sick children, breath-holding is often limited or not feasible. Sedation can facilitate breath-holding but is highly undesirable. For these reasons, there is a need to develop free-breathing MRI technology that accurately quantifies steatosis in all children.

Objective This study aimed to compare non-sedated free-breathing multi-echo 3-D stack-of-radial (radial) MRI versus standard breath-holding MRI and SVS techniques in a group of children for fat quantification with respect to image quality, accuracy and repeatability.

Materials and methods Healthy children (n=10, median age [±interquartile range]: 10.9 [±3.3] years) and overweight children with nonalcoholic fatty liver disease (NAFLD) (n=9, median age: 15.2 [±3.2] years) were imaged at 3 Tesla using free-breathing radial MRI, breath-holding Cartesian MRI and breath-holding SVS. Acquisitions were performed twice to assess repeatability (within-subject mean difference, MD_{within}). Images and hepatic proton-density fat fraction (PDFF) maps were scored for image quality. Free-breathing and breath-holding PDFF were compared using linear regression (correlation coefficient, r and concordance correlation coefficient, ρ_c) and Bland-Altman analysis (mean difference). P<0.05 was considered significant.

Results In patients with NAFLD, free-breathing radial MRI demonstrated significantly less motion artifacts compared to breath-holding Cartesian (P<0.05). Free-breathing radial PDFF demonstrated a linear relationship (P<0.001) versus breath-holding SVS PDFF and breath-holding Cartesian PDFF with r=0.996 and ρ_c=0.994, and r=0.997 and ρ_c=0.995, respectively. The mean difference in PDFF between free-breathing radial MRI, breath-holding Cartesian MRI and breath-holding SVS was <0.7%. Repeated free-breathing radial MRI had MD_{within}=0.25% for PDFF.

Conclusion In this pediatric study, non-sedated free-breathing radial MRI provided accurate and repeatable hepatic PDFF measurements and improved image quality, compared to standard breath-holding MR techniques.

Keywords Children · Fat · Liver · Magnetic resonance imaging · Nonalcoholic fatty liver disease · Quantification · Radial multi-echo sequence

✉ Holden H. Wu
holdenwu@mednet.ucla.edu

[1] Department of Radiological Sciences, David Geffen School of Medicine, University of California Los Angeles, Los Angeles, CA, USA

[2] Physics and Biology in Medicine, University of California Los Angeles, Los Angeles, CA, USA

[3] Department of Pediatrics, Division of Neonatology, David Geffen School of Medicine, University of California Los Angeles, Mattel Children's Hospital, Los Angeles, CA, USA

Introduction

Nonalcoholic fatty liver disease (NAFLD) is the accumulation of hepatic fat in the absence of excessive alcohol intake when other liver disorders have been excluded. In the United States, 12.7 million children are obese [1] and 38% of obese children have NAFLD [2]. NAFLD can progress to nonalcoholic steatohepatitis, which can lead to cirrhosis, hepatocellular carcinoma and liver failure [3–5]. Liver biopsy is the gold standard for diagnosing and staging NAFLD [6, 7]. However, biopsies are invasive, limited by sampling bias, require anesthesia and can be associated with complications. Biopsies are also technically challenging [8, 9], particularly in obese children. Complicating matters, interobserver agreement among pathologists for NAFLD scoring can be variable [9–11]. For these reasons, there is a need for a noninvasive technique to accurately measure hepatic fat in children.

In adults, noninvasive magnetic resonance (MR) techniques have been developed to quantify hepatic fat. MR spectroscopy is regarded as a reference standard for noninvasive fat quantification [12, 13] and accurately quantifies hepatic steatosis [14–16]. However, MR spectroscopy only measures fat content in a single spatial location (i.e. voxel) and is limited by spatial sampling bias [12, 13]. Magnetic resonance imaging (MRI) is noninvasive and achieves spatially resolved hepatic fat quantification in 2-D slices or 3-D volumes by using chemical shift encoded (CSE) methods to calculate proton-density fat fraction (PDFF) [17–19]. To obtain accurate PDFF quantification, confounding factors such as complexities in the fat spectral model, T_1 and T_2^* bias, gradient delay and eddy current errors, and noise bias must be considered [20]. CSE-MRI methods have mainly been investigated in adults with a few studies in children [19, 21–23]. In adults, CSE-MRI PDFF accurately detects and quantifies hepatic steatosis when compared to MR spectroscopy [24] and liver biopsy [25, 26].

Conventional MRI techniques, including CSE-MRI methods [24, 27–29], typically employ Cartesian trajectories for MR image acquisition [29–31]. Cartesian trajectories are limited by their sensitivity to respiratory motion-induced coherent aliasing artifacts, which degrade image quality and negatively impact PDFF quantification. In an attempt to compensate for this limitation, Cartesian MRI acquisitions of the liver are performed during a breath-hold. Because imaging parameters are selected to reduce scan times to fit within a breath-hold (typically 10 to 20 s), flexibility in acquiring larger spatial coverage, higher resolution, and/or greater signal-to-noise ratio (SNR) may be limited.

Additionally, a breath-hold is limited or not feasible in many patients (adults and children), specifically those with disabilities, neurological disorders, chronic illnesses, difficulties with communication or those unable to comply with operator instructions [29–31]. Even when children are able to suspend respiration, inconsistency and reduced breath-hold capacity compromise diagnostic information. While respiratory gating and self-navigation strategies for Cartesian MRI sequences can be used to mitigate motion artifacts, these strategies require longer and potentially variable scan times, and image quality may still suffer [29, 32, 33]. For these reasons, children may be sedated for abdominal MRI scans. However, sedation can have negative side effects and complications, particularly in children [31, 34]. As a result, there is a need for new free-breathing MRI techniques that overcome the challenges of traditional breath-hold MRI and avoid the need for sedation.

Non-Cartesian trajectories provide an alternative for MR imaging in children that eliminates the need for a breath-hold and sedation. Non-Cartesian 3-D stack-of-radial trajectories (also known as stack-of-stars) have dispersed motion artifacts in the radial encoding direction (in-plane) that do not obscure the anatomy, making radial trajectories more robust to breathing motion [29–31, 35–37]. As a result, radial MRI scans can be acquired during free-breathing, allowing for greater liver coverage, higher spatial resolution, and/or increased SNR. Recently, a new free-breathing multi-echo 3-D stack-of-radial MRI technique (free-breathing radial) with gradient error calibration and correction was developed for PDFF quantification in adults [36]. This technique acquires MRI data continuously during a free-breathing scan, reconstructs images and calculates PDFF maps. In adults, the hepatic PDFF measurements generated by free-breathing radial demonstrated a high degree of quantitative agreement to standard breath-hold MR spectroscopy and CSE-MRI techniques [36]. However, to date, there is no research on free-breathing hepatic fat quantification in children. Accordingly, this study's purpose is to compare the image quality, accuracy and repeatability of this free-breathing radial technique [36] to conventional breath-hold MRI and breath-hold MR spectroscopy techniques for hepatic fat quantification in children.

Materials and methods

Pediatric study population

This study was approved by our local institutional review board. Parents/legal guardians provided informed consent and children provided assent. Healthy children and children with NAFLD, ages 7-17 years, were enrolled. Exclusion criteria included known liver disease (excluding NAFLD for NAFLD patients), infections, diseases or congenital anomalies known to affect the liver, contraindications to MRI and an inability to comply with breath-holding instructions.

Pediatric liver MR experiments

MRI experiments were performed on a 3-T scanner (MAGNETOM Skyra or Prisma; Siemens, Erlangen,

Germany) using a spine array coil and body matrix array. Sequences acquired during the scan included a commercially available breath-holding 3-D Cartesian CSE-MRI sequence with controlled aliasing in parallel imaging results in higher acceleration (CAIPIRINHA) reconstruction (qDixon, the LiverLab package, software version VE11; Siemens, Erlangen, Germany), a commercially available breath-holding stimulated echo acquisition mode single-voxel MR spectroscopy (SVS) sequence (HISTO, the LiverLab package, software version VE11; Siemens, Erlangen, Germany), and a free-breathing radial sequence [28, 36, 39, 40]. Each sequence was repeated for each patient in random order within each scan session to evaluate repeatability. Except for the acceleration factor and the number of slices, the same imaging parameters were used for breath-holding Cartesian and free-breathing radial to enable a fair comparison between techniques (Table 1). The SVS voxel size was 25 mm × 25 mm × 25 mm with a total acquisition time of 15 s. SVS imaging parameters included echo times of 12 ms, 24 ms, 36 ms, 48 ms and 72 ms, a repetition time of 3,000 ms, a mixing time of 10 ms, a vector size of 1,024, and a bandwidth of 1,200 Hz/pixel. Additional MRI scans were repeated if motion artifacts resulted in nondiagnostic images. The breath-holding SVS region of interest (ROI) was positioned to avoid regions with image artifacts on breath-holding Cartesian, large blood vessels and bile ducts.

Table 1 Representative sequence parameters for in vivo pediatric liver experiments

Imaging parameters	BH Cartesian	FB radial
TE (ms)	1.23, 2.46, 3.69, 4.92, 6.15, 7.38	1.23, 2.46, 3.69, 4.92, 6.15, 7.38
ΔTE (ms)	1.23	1.23
TR (ms)	8.85	8.85
Matrix (N_x×N_y)	160-288×160-288	160-288×160-288
Field of view (mm_x×mm_y)	280-500×280-500	280-500×280-500
Resolution (mm_x×mm_y)	1.67-1.94×1.67-1.94	1.67-1.94×1.67-1.94
Slice thickness (mm)	5	5
Number of slices	20-40	36-52
Radial spokes	N/A	252-453◆
Flip angle (degrees)	5	5
Bandwidth (Hz/pixel)	1,080-1,160	1,080-1,160
Acceleration factor	4	1
Scan time (min:s)	0:16-0:25	2:09*-4:43*

A slice-oversampling factor of 18-25% was used for the acquisitions. Imaging parameters for free-breathing (FB) radial and breath-holding (BH) Cartesian scans were matched as much as possible for each subject. The number of slices was adjusted depending on scan time and the subjects' breath-holding ability

TE echo time, *TR* repetition time

*The free-breathing radial gradient calibration scan time (31-45 s) is included

◆Based on Nyquist criteria to collect fully sampled data with N_x×π/2 spokes

MR image reconstruction and PDFF calculation

Breath-holding Cartesian acquisitions were reconstructed and PDFF maps were determined by a prototype scanner software (Work-In-Progress package 963, software version VE11; Siemens, Erlangen, Germany) [28]. The breath-holding Cartesian PDFF maps were calculated using a 7-peak fat model and single effective R_2^* per voxel; breath-holding SVS PDFF was calculated by the scanner software using T_2 correction [28, 40, 41]. Free-breathing radial data sets (fully sampled based on Nyquist criteria) were reconstructed, without discarding data or employing parallel imaging reconstruction techniques. Free-breathing radial PDFF maps were calculated offline in MATLAB R2016a (MathWorks, Natwick, MA, USA) using the same signal model used for breath-holding Cartesian PDFF maps, complex fitting with a graph cut algorithm, and magnitude discrimination [36, 41–45].

Image analysis

All reconstructed images and PDFF maps were converted to DICOM (Digital Imaging and Communications in Medicine) for analysis in OsiriX software version 6.0 (Pixmeo Sarl, Bernex, Switzerland). Image quality was evaluated by an experienced pediatric radiologist (S.G., >10 years of experience) masked to the trajectory (Cartesian or radial) and patient, by scoring the first echo time images (TE=1.23 ms) and PDFF maps in axial and coronal orientations. Images were scored on a scale of 1-4 for motion artifacts, other imaging artifacts and image blurring. Motion artifacts included coherent aliasing artifacts on breath-holding Cartesian images and radial streaking on free-breathing radial images. Other artifacts included CAIPIRINHA reconstruction artifacts on breath-holding Cartesian images and any additional non-motion-related artifacts on breath-holding Cartesian and free-breathing radial images. Motion blurring referred to the blurring of blood vessels, abdominal wall or liver dome on breath-holding Cartesian and free-breathing radial images. The criteria for a score of 1 were nondiagnostic images with significant artifacts that confound PDFF (i.e. bad image quality); 2 indicated diagnostic images with artifacts that confound PDFF, 3 indicated diagnostic images with artifacts that did not confound PDFF and 4 indicated no artifacts (i.e. good image quality). The percentage of images that fell into each score category was determined. To characterize liver coverage, the number of slices that contained the liver using the breath-holding Cartesian scan (Nsl_C) and the free-breathing radial scan (Nsl_R) was counted. Free-breathing radial scans were always prescribed to cover the entire liver. The liver slice coverage (Lsl) was then calculated as the percentage of liver slices

covered using breath-holding Cartesian relative to free-breathing radial (i.e. $Lsl=Nsl_C/Nsl_R\times100\%$) and reported as mean±standard deviation (SD). To evaluate quantitative hepatic PDFF accuracy, one ROI was drawn on each of the breath-holding Cartesian and free-breathing radial PDFF maps in an anatomical location corresponding to the breath-holding SVS ROI that was placed during the MR scan, and PDFF was recorded as mean±SD.

Statistical analysis

Age was described for healthy subjects and patients with NAFLD and the median values and interquartile range (IQR) were compared using a nonparametric two group Mann-Whitney *U* test due to the limited sample size [46, 47]. Paired differences in image quality scores between breath-holding Cartesian (i.e. conventional reference) and free-breathing radial scans, were assessed using McNemar-Bowker tests for dependent categorical data to compare the distribution of scores by cohort (healthy cohort vs. NAFLD cohort) and artifact category (motion artifacts, other artifacts and motion blurring) [48].

Simple linear regression analysis was performed to compare techniques by determining the equation for the linear relationship, Pearson's correlation coefficient (r) and Lin's concordance correlation coefficient (ρ_c) [49, 50]. Pearson's r was calculated to evaluate the strength of the linear associations between the two techniques, whereas Lin's ρ_c was calculated to estimate the degree of quantitative agreement (i.e. to estimate whether free-breathing radial or breath-holding techniques produce the exact same value for the range of hepatic PDFF). For example, when two techniques produce the exact same hepatic PDFF, ρ_c is 1. Lin's ρ_c was reported in this study because a high Pearson's r does not necessarily imply identical measurements between free-breathing radial and breath-holding techniques. The equation for the concordance coefficient comparing free-breathing radial to breath-holding techniques is shown in the Appendix. Bland-Altman analysis was performed to assess differences between two techniques by plotting the PDFF difference between the two techniques against the mean PDFF between the two techniques [51]. Specifically, the Bland-Altman analysis measures the mean difference (MD) or bias between two methods and the 95% limits of agreement (LoA), which were reported as mean difference (MD)±1.96 times the SD (i.e. $\pm LoA=MD\pm1.96\times SD$).

To assess repeatability for each technique, the within-subject mean difference (MD_{within}), within-subject SD (SD_{within}) and within-subject coefficient of repeatability (CR_{within}) between repeated scans were reported [52, 53]. The CR_{within} measures the variability for repeated measurements of the same technique (i.e. $CR_{within}=1.96\times\sqrt{2}\times SD_{within}$), therefore a smaller CR_{within} demonstrates smaller differences between repeated measurements [53]. Statistical analyses were performed in STATA software version 12.0 (Statacorp, College Station, TX) and MATLAB. A *P*-value <0.05 was considered significant.

Results

Pediatric study population

Ten healthy subjects and ten patients with NAFLD were enrolled. Of these, all ten healthy subjects (6 male, median age [±IQR]: 10.9 [±3.3] years) and 9 NAFLD patients (7 male, age: 15.2 [±3.2] years) completed the study. The median age between the two groups was significantly different ($P<0.05$). One patient with NAFLD did not complete the study because the MRI field of view was not adequate to cover his/her body habitus. All of the patients with NAFLD were confirmed by breath-holding SVS or breath-holding Cartesian to have hepatic PDFF >5.6%, consistent with a diagnosis of NAFLD [14, 54].

Image quality

If the breath-holding Cartesian images showed significant aliasing artifacts due to motion or if the breath-holding liver position changed such that the images from the breath-holding Cartesian scan did not adequately cover the liver volume, breath-holding Cartesian scan(s) were repeated. For some subjects, motion-induced aliasing or other artifacts were still observed on breath-holding Cartesian images even when repeated. The number of repeated breath-holding Cartesian scans ranged from 0 to 2 for all subjects. Specifically, the mean number of repeated breath-holding Cartesian scans performed was 0.40±0.70 in healthy subjects and 0.89±0.93 in patients with NAFLD. In contrast, the free-breathing radial scan was only repeated once for one healthy subject.

The free-breathing radial technique demonstrated robustness to motion with good image quality and quantitative PDFF maps. Representative images of breath-holding Cartesian and free-breathing radial acquisitions with motion artifact image quality scores ranging from 1 to 4 are shown in Fig. 1. Figure 2 shows an example of breath-holding Cartesian and free-breathing radial images and PDFF maps from a representative subject where major and minor motion occurred during a breath-holding Cartesian scan.

Axial, reformatted coronal and reformatted sagittal PDFF maps from free-breathing radial and breath-holding Cartesian techniques for a representative healthy subject and patient with NAFLD are shown in Figs. 3 and 4, respectively. The PDFF maps from free-breathing radial scans and breath-holding Cartesian scans are similar, but have slight differences in liver position due to the breath-holding. Additionally, in some NAFLD patients hepatic PDFF heterogeneity was observed

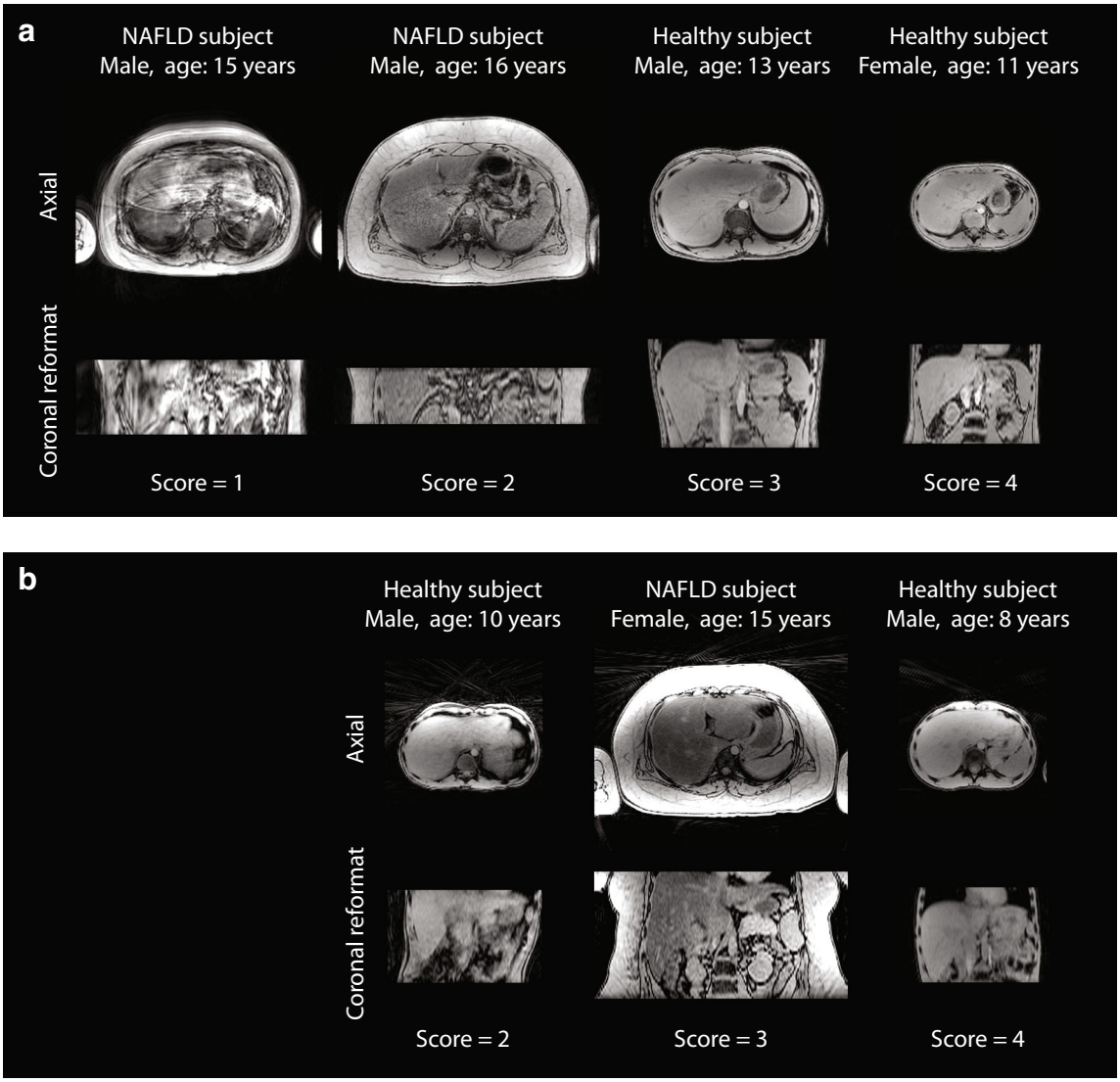

Fig. 1 Representative images in axial and coronal reformat orientations at an echo time of 1.23 ms with motion artifact scores of 1-4 for (**a**) breath-holding Cartesian and 2-4 for (**b**) free-breathing radial acquisitions. If the breath-holding Cartesian acquisition exhibited severe motion artifacts leading to nondiagnostic images (score of 1), additional scans were repeated during the scan session. The free-breathing radial acquisition did not have a representative image with an image quality score of 1. See Materials and methods for the description of the image quality scores

using both breath-holding Cartesian and free-breathing radial techniques (Fig. 5).

In healthy subjects, the breath-holding Cartesian scan achieved full liver slice coverage with the resolution used in this study. However, in most patients with NAFLD, full liver slice coverage was not achieved using the breath-holding Cartesian technique. In patients with NAFLD, the liver slice coverage was 100%±0% for free-breathing radial scans while it was 74%±17% for breath-holding Cartesian scans. To maintain similar resolution among all subjects, many NAFLD patients required a larger matrix size than healthy subjects due to a larger field of view. Furthermore, some patients with NAFLD had limited breath-holding ability and the volumetric coverage needed to be reduced further to decrease the breath-holding time. Table 2 shows that for patients with NAFLD, free-breathing radial scans had a significantly higher proportion of good motion artifact and other artifact image quality scores compared to breath-holding Cartesian scans ($P<0.05$). In both patients with NAFLD and healthy subjects, the proportion of image blurring scores was not significantly different between free-breathing radial scans and breath-holding Cartesian scans.

Hepatic PDFF quantification accuracy

To avoid PDFF errors due to coherent Cartesian aliasing artifacts, all ROIs measured using the breath-holding SVS, free-breathing radial images, and breath-holding Cartesian images

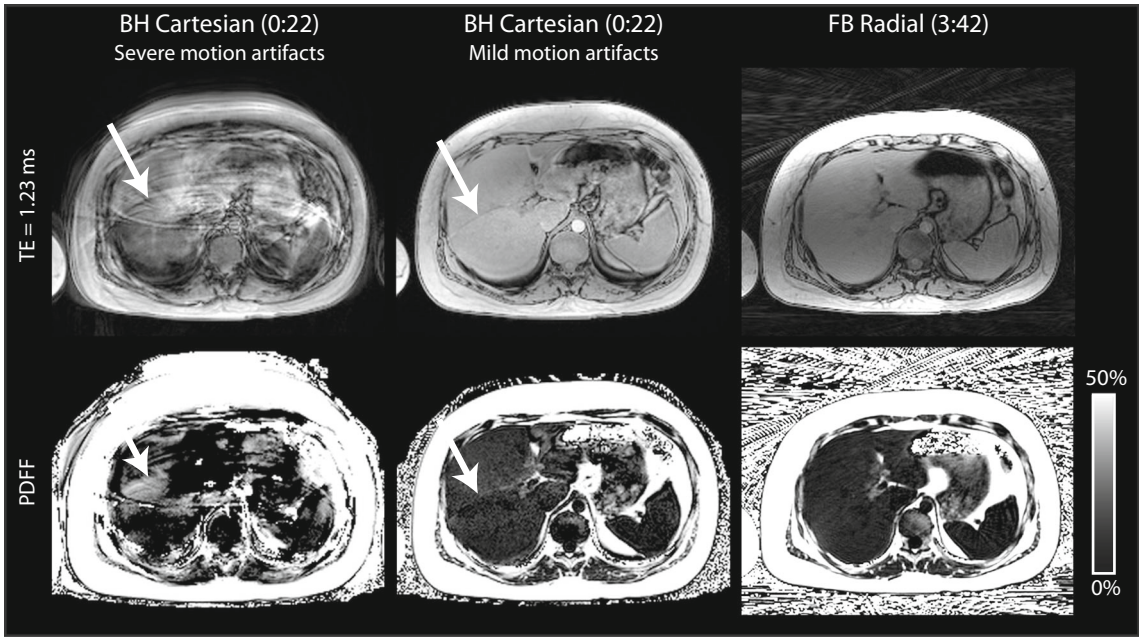

Fig. 2 Images and proton-density fat fraction (PDFF) maps for the free-breathing radial and breath-holding Cartesian scans for a representative NAFLD patient (15-year-old boy) in axial orientation. Due to severe motion artifacts (nondiagnostic image quality) in the breath-holding Cartesian scan (motion artifact score=1), it was repeated. However, mild motion artifacts (motion artifact score=3) were still present in the repeated scan. Arrows indicate artifacts that affect hepatic fat quantification. The free-breathing radial scan did not exhibit coherent motion artifacts in the liver (motion artifact score=3). The scan time for each technique is reported as minutes:seconds

were positioned away from Cartesian MRI artifacts for quantitative analysis. The results showed a linear relationship between breath-holding Cartesian PDFF, breath-holding SVS PDFF and the proposed free-breathing radial PDFF. All comparisons had a significant r and ρ_c >0.99 (P<0.001) and MD <0.7%. The linear correlation and Bland-Altman plots are shown in Fig. 6. The comparison between the proposed free-breathing radial PDFF versus breath-holding Cartesian PDFF showed a slope of 1.03 for the linear regression and correlation coefficients r and ρ_c were 0.996 and 0.994, respectively. For the proposed free-breathing radial PDFF versus breath-holding SVS PDFF, the slope for the linear regression was 0.97 and the

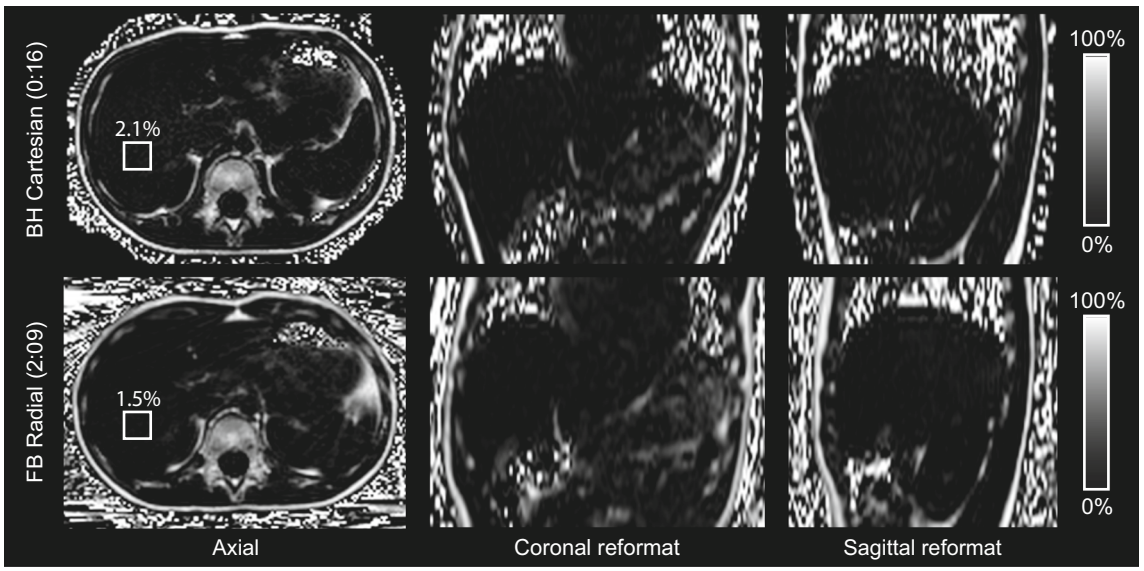

Fig. 3 Proton-density fat fraction (PDFF) maps for breath-holding Cartesian and free-breathing radial scans for a representative healthy subject (9-year-old boy) in axial, coronal and sagittal orientations. The liver slice coverage was 100% using the breath-holding Cartesian technique. Representative regions of interest (*boxes*) and mean PDFF values are shown in the axial orientation. Free-breathing radial and breath-holding Cartesian scans have slight differences in liver position due to breath-holding. The scan time for each technique is reported as minutes:seconds

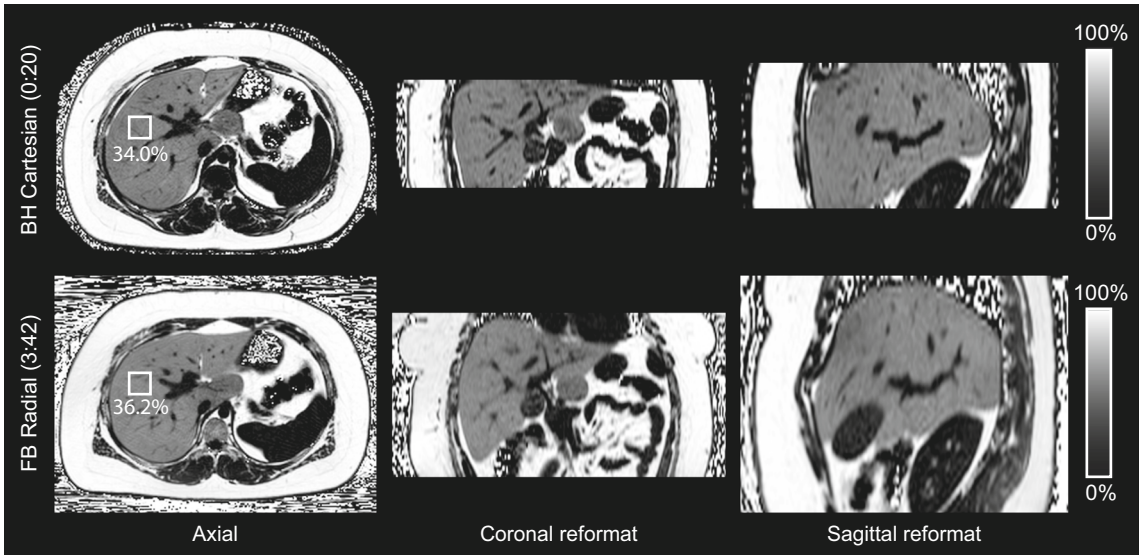

Fig. 4 Proton-density fat fraction (PDFF) maps for breath-holding Cartesian and free-breathing radial scans for a representative nonalcoholic fatty liver disease (NAFLD) patient (14-year-old girl) in axial, coronal and sagittal orientations. The liver slice coverage was 68% using the breath-holding Cartesian technique. Representative regions of interest (*boxes*) and mean PDFF values are shown in the axial orientation. Free-breathing radial and breath-holding Cartesian scans have slight differences in liver position due to breath-holding. The scan time for each technique is reported as minutes:seconds

correlation coefficients r and ρ_c were 0.997 and 0.995, respectively. The conventional breath-holding Cartesian PDFF versus the reference breath-holding SVS PDFF comparison showed a slope for the linear regression of 0.94 and the correlation coefficients r and ρ_c were 0.997 and 0.995, respectively. The mean difference between free-breathing radial PDFF and conventional breath-holding Cartesian PDFF was 0.65%±2.56%, the mean difference between free-breathing radial PDFF and reference breath-holding SVS PDFF was 0.64%±2.31%, and the mean difference between conventional breath-holding Cartesian PDFF and reference breath-holding SVS PDFF was 0.23%±2.56%. Free-breathing radial PDFF, breath-holding

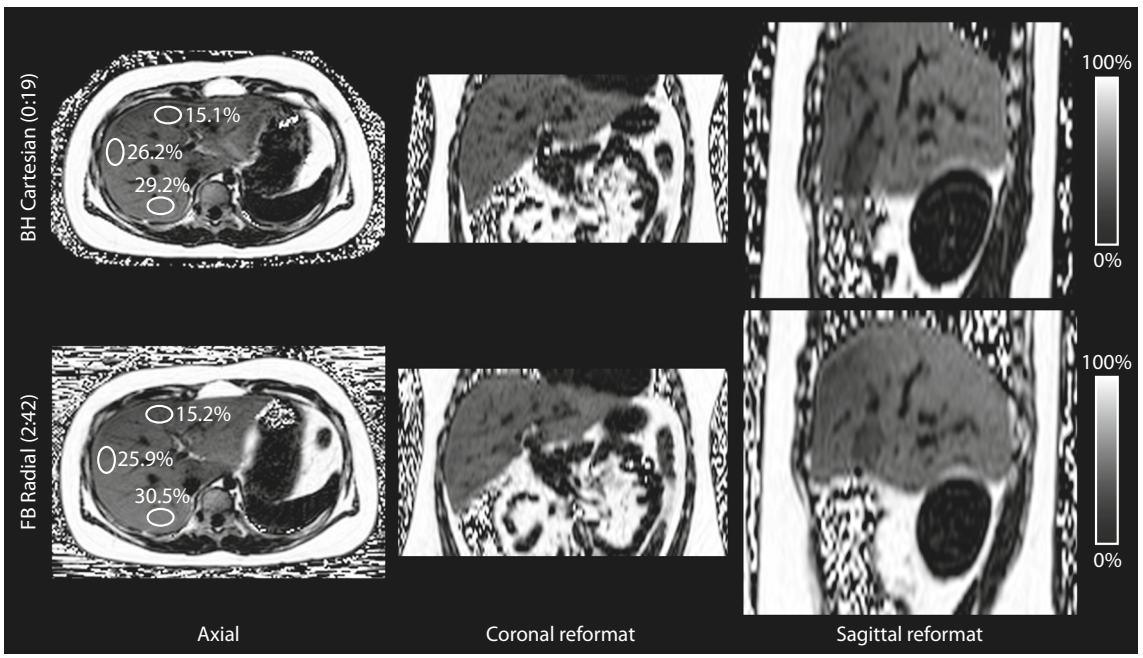

Fig. 5 Proton-density fat fraction (PDFF) maps for breath-holding Cartesian and free-breathing radial scans for a representative nonalcoholic fatty liver disease (NAFLD) patient (10-year-old boy) with hepatic PDFF heterogeneity in axial, coronal and sagittal orientations. The liver slice coverage was 97% using the breath-holding Cartesian technique. Representative regions of interest (*circles*) and mean PDFF values are shown in three liver segments. Free-breathing radial and breath-holding Cartesian scans have slight differences in liver position due to breath-holding. The scan time for each technique is reported as minutes:seconds

Table 2 Radiologist image quality scores for the breath-holding (BH) Cartesian and free-breathing (FB) radial first echo time images and proton density fat fraction (PDFF) maps for motion artifacts, other artifacts, and image blurring for the healthy pediatric subjects and nonalcoholic fatty liver disease (NAFLD) pediatric patients. Images were scored on a scale of 1–4 where a score of 1 indicates bad image quality and 4 indicates good image quality

	Healthy subjects (n=10)		NAFLD patients (n=9)	
Motion artifacts	BH Cartesian*	FB radial*	BH Cartesian*	FB radial*
1 (bad)	0%	0%	0%	0%
2	0%	5%	56%	11%
3	40%	80%	28%	83%
4 (good)	60%	15%	17%	6%
Other artifacts	BH Cartesian	FB radial	BH Cartesian*	FB radial*
1 (bad)	0%	0%	0%	0%
2	0%	0%	61%	0%
3	70%	85%	33%	89%
4 (good)	30%	15%	6%	11%
Image blurring	BH Cartesian	FB radial	BH Cartesian	FB radial
1 (bad)	0%	0%	0%	0%
2	0%	0%	0%	0%
3	60%	85%	50%	44%
4 (good)	40%	15%	50%	56%

*Statistically significant differences (P<0.05) in the distribution of image quality scores between BH Cartesian and FB radial techniques

Cartesian PDFF and breath-holding SVS PDFF demonstrated repeatability with MD_{within}=0.25%, -0.09% and -0.30%, respectively; SD_{within}=0.55%, 0.32% and 1.35%, respectively; CR_{within}=1.53%, 0.89% and 3.74%, respectively. A summary of the repeatability analysis is shown in Table 3.

Discussion

In this study, we evaluated the accuracy and repeatability of 3-D hepatic PDFF quantification using a free-breathing radial MRI technique with respect to established breath-holding techniques in a pediatric population. This study provides evidence that accurate and repeatable free-breathing hepatic fat quantification can be performed in children for the entire 3-D liver volume using a multi-echo 3-D stack-of-radial technique. Hepatic PDFF calculated from free-breathing radial scans had significant linear correlation, significant concordance and low mean differences <0.7% compared to the conventional breath-holding Cartesian and the reference standard breath-holding SVS techniques. Free-breathing radial, breath-holding Cartesian and breath-holding SVS techniques demonstrated repeatability with MD_{within}<0.3%. Free-breathing radial scans and breath-holding Cartesian scans demonstrated repeatability with CR_{within}<2%. Breath-holding SVS scans had a larger CR_{within} of 3.74% likely due to variation in the breath-holding position and actual voxel position between breath-holding SVS scans. While the mean PDFF differences between free-breathing radial and breath-holding techniques were very small, they may reflect differences due to the breath-holding position, SVS partial volume effects and the effect of motion on the images. Importantly, in patients with NAFLD, free-breathing radial scans demonstrated a significantly higher proportion of good image quality scores compared with breath-holding Cartesian scans. We speculate that overweight patients with NAFLD may have had more difficulty performing a breath-hold than their healthy peers. The median (±IQR) body mass index in the NAFLD cohort was 33.2 (±7.1) kg/m^2. In contrast, the body mass index in the healthy cohort was normal at 17.4 (±2.0) kg/m^2. Therefore, compared to the conventional breath-holding Cartesian technique, free-breathing radial scans may provide improved image quality and hepatic PDFF quantification for evaluating steatosis in this target population.

There have been a few studies evaluating breath-holding Cartesian CSE-MRI techniques for hepatic PDFF quantification in children [19, 21–23]. Two studies used dual-echo and triple-echo methods for PDFF quantification [21, 23]. However, dual-echo and triple-echo approaches do not correct for all confounding factors (such as T_2* bias and the multi-peak spectrum of fat) and, as a result, hepatic PDFF quantification may be inaccurate [20]. Since the signal model includes many parameters, at least four echoes are recommended to account for confounding factors such as T_2* bias and the multi-peak spectrum of fat (e.g., not correcting for T_2* can cause an underestimated hepatic fat fraction) [20, 55]. Other studies utilized a six-echo technique with magnitude-based fitting for PDFF estimation in the liver and found agreement between breath-holding Cartesian PDFF and breath-holding

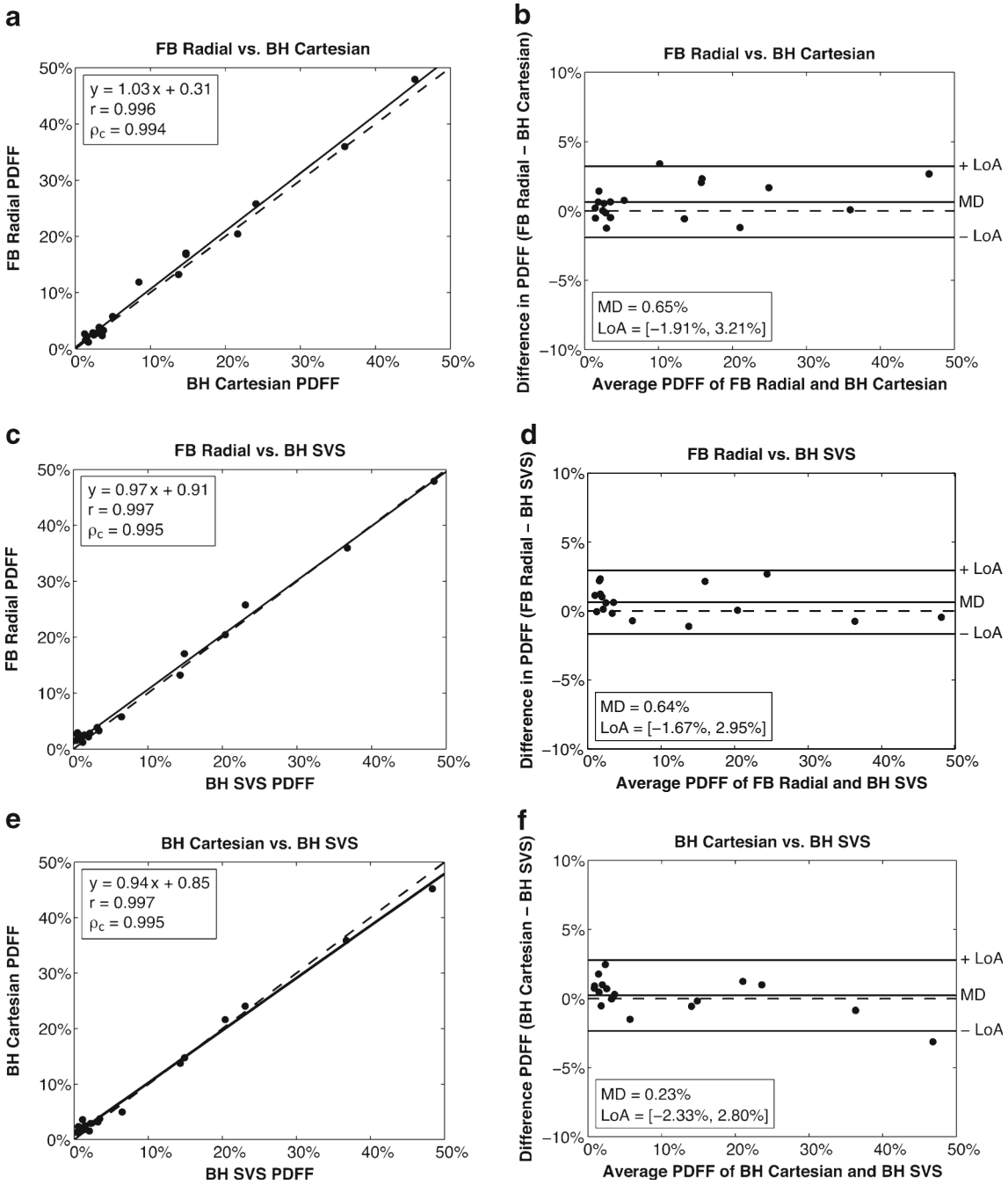

Fig. 6 Liver study (**a, c, e**) linear correlation plots and (**b, d, f**) Bland-Altman plots for proton-density fat fraction (PDFF) of each region of interest (ROI) in the liver corresponding to the single-voxel magnetic resonance spectroscopy (SVS) ROI. The comparison of (**a-b**) free-breathing radial versus breath-holding Cartesian had mean difference =0.65%±2.56% (**c-d**) free-breathing radial versus breath-holding SVS had mean difference =0.64%±2.31%, and (**e-f**) breath-holding Cartesian versus breath-holding SVS had mean difference=0.23%±2.56%. The correlation coefficients r and ρ_c were significant in all cases with $P<0.001$. The dashed lines represent y=x in the linear correlation plots and y=0 in the Bland-Altman plots. *BH* breath-holding, *FB* free-breathing

SVS PDFF, correlation between breath-holding Cartesian PDFF and histopathology, and associations between breath-holding Cartesian PDFF and clinical characteristics [19, 22, 23]. These studies employed a 2-D breath-holding Cartesian MRI technique, which may have limited spatial coverage or resolution and motion artifacts [19, 21–23].

In this study, variation in the distribution of image quality scores between breath-holding Cartesian and free-breathing radial was dependent upon the artifact category and subject population. Blurring was observed in breath-holding Cartesian and free-breathing radial images with no statistically significant differences in the distribution of scores for both

Table 3 The analysis of repeatability results. The within-subject mean difference (MD_{within}), within-subject standard deviation (SD_{within}), and within-subject coefficient of repeatability (CR_{within}) are reported between repeated scans for the breath-holding (BH) single-voxel magnetic resonance spectroscopy (SVS), BH Cartesian and free-breathing (FB) radial techniques

Technique	MD_{within} (%)	SD_{within} (%)	$CR_{within}=1.96\times\sqrt{2}\times SD_{within}$(%)
FB radial	0.25	0.55	1.53
BH Cartesian	-0.09	0.32	0.89
BH SVS	-0.30	1.35	3.74

healthy subjects and patients with NAFLD. This did not affect PDFF quantification. In the motion artifact category, breath-holding Cartesian images had coherent aliasing artifacts that may confound hepatic PDFF while free-breathing radial images had radial streaking artifacts that interfere less with hepatic PDFF. In patients with NAFLD, the percentage of bad image quality scores for motion artifacts was higher for the breath-holding Cartesian technique than for the free-breathing radial technique. We believe this is because children with NAFLD may have difficulty performing a breath-hold due to impaired lung function secondary to their overweight/obese status. Additionally, in patients with NAFLD, breath-holding Cartesian scans showed a higher percentage of bad image quality scores for other artifacts. One of the main sources of these artifacts is related to undersampling and CAIPIRINHA reconstruction errors. This is most likely due to the fact that the center of the field of view's coil sensitivity is reduced by a large body size. In order to improve breath-holding Cartesian image quality for patients with NAFLD, less undersampling may be required, which would increase scan time, reduce volumetric coverage and/or reduce spatial resolution. On the other hand, the free-breathing radial technique does not necessarily require parallel imaging or have breath-holding scan time limitations. Therefore, image quality can be improved by allowing for longer free-breathing acquisition times for patients with NAFLD.

In this study, the breath-holding Cartesian technique required four-fold undersampling to reduce the scan time to within a breath-hold. For this reason, volumetric coverage was limited. As a result, for children with hepatomegaly, full liver slice coverage with the desired spatial resolution may not be achievable within a breath-hold. Free-breathing radial scans can achieve greater volumetric coverage and/or spatial resolution compared to breath-holding Cartesian scans, thereby improving 3-D spatial characterization of hepatic PDFF and liver disease. This may be important for cases where hepatic PDFF is heterogeneous (Fig. 5). Other studies have reported heterogeneous hepatic PDFF in adults and children, and recent evidence suggests heterogeneity in liver fat reduction following bariatric surgery [56–60]. However, additional studies are required for a full understanding of the spatial distribution of PDFF in patients with NAFLD. In addition, full liver coverage achieved by free-breathing radial MRI may have additional clinical applications including the evaluation of hepatic masses or other diseases. Traditionally, complex hepatic diseases require sedation or general anesthesia for MRI in order ensure full liver coverage and adequate resolution. Free-breathing radial MRI technology eliminates this requirement, and at the same time can yield diagnostically useful information. Each free-breathing radial acquisition in this study was performed with the same image resolution for children with either a small or large body habitus, and the number of slices was chosen to cover the entire liver volume. For these reasons, fully sampled free-breathing radial acquisitions were approximately 2-5 min depending upon the subject's size (Table 1). The free-breathing radial scan time could be shortened if fewer slices are acquired or a lower resolution is used. On the other hand, higher resolutions may improve diagnostic information when performing MRI scans, but this may require longer scan times or reduced liver slice coverage. While the radial trajectory was fully sampled in this study, radial undersampling can be performed in combination with non-Cartesian parallel imaging reconstruction [61]. Previous work in adults showed similar PDFF quantification results using an undersampled free-breathing radial technique, potentially reducing the scan time to less than 1.5 min [36].

In addition to the constraints of the breath-holding Cartesian technique with respect to liver coverage and spatial resolution, patient motion leads to artifacts and reduces image quality. Previous studies have developed respiratory gating and self-navigation strategies for hepatic fat quantification using Cartesian MRI sequences to reduce motion artifacts in adults [32, 33]. To our knowledge, these strategies have not been evaluated for hepatic fat quantification in children. In adults, respiratory gating and self-navigation have shown similar image quality and fat quantification accuracy compared to breath-holding techniques [32, 33]. However, these strategies require longer scan times for image acquisition and are well-suited for patients with regular respiratory patterns, but may not be appropriate for children who require shorter scan times and have heavy or irregular breathing [29, 33]. In fact, respiratory gating and self-navigation strategies may benefit from the incorporation of non-Cartesian trajectories, such as 3-D stack-of-radial, to accommodate patients with heavy or irregular breathing. Although self-navigation using the free-breathing radial technique was not evaluated in this current

study, the 3-D stack-of-radial trajectory allows for self-navigation and improved image quality in the presence of motion [38, 62].

The signal model used in this study includes fitting for R_2^*, which can be used to assess hepatic iron content [63–66]. Severe hepatic iron overload may hinder PDFF quantification due to rapid signal decay prior to acquiring the first echo time [63]. To address this, recent work includes ultra-short echo time sequences for R_2^* mapping in patients with severe iron overload [67–69]. In this study, there were no subjects with severe iron overload. Therefore, hepatic PDFF quantification was not confounded by high R_2^* values.

Our study has limitations. First, partial-volume effects and motion can confound breath-holding SVS scans, which were not corrected. Second, inter-sequence motion and non-rigid changes in liver tissue during breath-holding and free-breathing may hinder PDFF comparisons between techniques. To address this limitation, ROIs were placed in corresponding anatomical locations on breath-holding Cartesian and free-breathing radial PDFF maps. Third, the scan time for the radial acquisition is increased by 31-45 s due to the addition of a calibration scan for radial MRI, and the number of radial read-outs needed for calibration was not optimized to reduce scan time. Finally, the sample size is small and this study was performed at a single site. However, the results of this study indicate that free-breathing radial is not only comparable to conventional breath-holding MR techniques, but also has some additional advantages for hepatic fat quantification in children.

Conclusion

In this study of healthy children and children with NAFLD, free-breathing hepatic fat quantification using a new 3-D stack-of-radial MRI technique was accurate and repeatable. The free-breathing radial technique demonstrated significantly less image artifacts than breath-holding Cartesian scans in patients with NAFLD. These results show that the free-breathing radial technique may potentially improve pediatric patient compliance and 3-D spatially resolved characterization of hepatic steatosis. Moreover, in this study, free-breathing radial eliminated the need for breath-holding and did not require sedation for fat quantification. The free-breathing radial technique represents a promising tool that could help clinicians diagnose and manage children with NAFLD.

Acknowledgments The authors thank Aaron Scheffler, Dr. Joanna Yeh, Barbara Lee, Tammy Floore, Glen Nyborg and Sergio Godinez at University of California Los Angeles (UCLA) for their help with this project. This work acknowledges the use of the International Society of Magnetic Resonance in Medicine Fat-Water Toolbox (http://ismrm.org/workshops/FatWater12/data.htm).

Research reported in this publication was supported in part by a UCLA Radiology Department Exploratory Research Grant.

Compliance with ethical standards

Conflicts of interest T. Armstrong and H. H. Wu receive institutional research support from Siemens Healthineers.

Appendix

Lin's concordance coefficient (ρ_c) [50] for free-breathing radial compared to breath-holding (Cartesian and SVS) techniques:

$$\rho_c = \frac{2r\sigma_{BH}\sigma_{FB}}{\sigma_{BH}^2 + \sigma_{FB}^2 + (\mu_{BH} - \mu_{FB})^2}$$

μ_{BH} and μ_{FB} are the means and σ_{BH} and σ_{FB} are the standard deviations of the free-breathing radial and breath-holding techniques, respectively; r is the correlation coefficient between the free-breathing and breath-holding technique.

References

1. Centers for Disease Control and Prevention. Overweight and Obesity. https://www.cdc.gov/obesity/data/childhood.html. Accessed 20 Nov 2017
2. Schwimmer JB, Deutsch R, Kahen T et al (2006) Prevalence of fatty liver in children and adolescents. Pediatrics 118:1388–1393
3. Feldstein AE, Charatcharoenwitthaya P, Treeprasertsuk S et al (2009) The natural history of non-alcoholic fatty liver disease in children: a follow-up study for up to 20 years. Gut 58:1538–1544
4. Pardee PE, Lavine JE, Schwimmer JB (2009) Diagnosis and treatment of pediatric nonalcoholic steatohepatitis and the implications for bariatric surgery. Semin Pediatr Surg 18:144–151
5. Younossi ZM (2008) Review article: current management of non-alcoholic fatty liver disease and non-alcoholic steatohepatitis. Aliment Pharmacol Ther 28:2–12
6. Uppal V, Mansoor S, Furuya KN (2016) Pediatric non-alcoholic fatty liver disease. Curr Gastroenterol Rep 18:24
7. Della Corte C, Vajro P, Socha P et al (2014) Pediatric non-alcoholic fatty liver disease: recent advances. Clin Res Hepatol Gastroenterol 38:419–422
8. Tapper EB, Lok AS-F (2017) Use of liver imaging and biopsy in clinical practice. N Engl J Med 377:756–768
9. Sumida Y, Nakajima A, Itoh Y (2014) Limitations of liver biopsy and non-invasive diagnostic tests for the diagnosis of nonalcoholic fatty liver disease/nonalcoholic steatohepatitis. World J Gastroenterol 20:475–485
10. Ovchinsky N, Moreira RK, Lefkowitch JH et al (2012) Liver biopsy in modern clinical practice: a pediatric point-of-view. Adv Anat Pathol 19:250–262
11. Manning DS, Afdhal NH (2008) Diagnosis and quantitation of fibrosis. Gastroenterology 134:1670–1681
12. Loomba R, Sirlin CB, Schwimmer JB et al (2009) Advances in pediatric nonalcoholic fatty liver disease. Hepatology 50:1282–1293
13. Lee SS, Park SH (2014) Radiologic evaluation of nonalcoholic fatty liver disease. World J Gastroenterol 20:7392–7402

14. Szczepaniak LS, Nurenberg P, Leonard D et al (2005) Magnetic resonance spectroscopy to measure hepatic triglyceride content: prevalence of hepatic steatosis in the general population. Am J Physiol Endocrinol Metab 288:E462–E468
15. Bohte AE, van Werven JR, Bipat S et al (2011) The diagnostic accuracy of US, CT, MRI and H-1-MRS for the evaluation of hepatic steatosis compared with liver biopsy: a meta-analysis. Eur Radiol 21:87–97
16. Georgoff P, Thomasson D, Louie A et al (2012) Hydrogen-1 MR spectroscopy for measurement and diagnosis of hepatic steatosis. AJR Am J Roentgenol 199:2–7
17. Meisamy S, Hines CDG, Hamilton G et al (2011) Quantification of hepatic steatosis with T1-independent, T2-corrected MR imaging with spectral modeling of fat: blinded comparison with MR spectroscopy. Radiology 258:767–775
18. Hines CDG, Yu H, Shimakawa A et al (2009) T1 independent, T2* corrected MRI with accurate spectral modeling for quantification of fat: validation in a fat-water-SPIO phantom. J Magn Reson Imaging 30:1215–1222
19. Achmad E, Yokoo T, Hamilton G et al (2015) Feasibility of and agreement between MR imaging and spectroscopic estimation of hepatic proton density fat fraction in children with known or suspected nonalcoholic fatty liver disease. Abdom Imaging 40: 3084–3090
20. Reeder SB, Cruite I, Hamilton G et al (2011) Quantitative assessment of liver fat with magnetic resonance imaging and spectroscopy. J Magn Reson Imaging 34:729–749
21. Koh H, Kim S, Kim MJ et al (2015) Hepatic fat quantification magnetic resonance for monitoring treatment response in pediatric nonalcoholic steatohepatitis. World J Gastroenterol 21:9741–9748
22. Schwimmer JB, Middleton MS, Behling C et al (2015) Magnetic resonance imaging and liver histology as biomarkers of hepatic steatosis in children with nonalcoholic fatty liver disease. Hepatology 61:1887–1895
23. Joshi M, Dillman JR, Singh K et al (2017) Quantitative MRI of fatty liver disease in a large pediatric cohort: correlation between liver fat fraction, stiffness, volume, and patient-specific factors. Abdom Radiol. https://doi.org/10.1007/s00261-017-1289-y
24. Bashir MR, Zhong X, Nickel MD et al (2015) Quantification of hepatic steatosis with a multistep adaptive fitting MRI approach: prospective validation against MR spectroscopy. AJR Am J Roentgenol 204:297–306
25. Kühn J-P, Hernando D, Muñoz del Rio A et al (2012) Effect of multipeak spectral modeling of fat for liver iron and fat quantification: correlation of biopsy with MR imaging results. Radiology 265:133–142
26. Idilman IS, Aniktar H, Idilman R et al (2013) Hepatic steatosis: quantification by proton density fat fraction with MR imaging versus liver biopsy. Radiology 267:767–775
27. Yokoo T, Shiehmorteza M, Hamilton G et al (2011) Estimation of hepatic proton-density fat fraction by using MR imaging at 3.0 T. Radiology 258:749–759
28. Zhong X, Nickel MD, Kannengiesser SAR et al (2014) Liver fat quantification using a multi-step adaptive fitting approach with multi-echo GRE imaging. Magn Reson Med 72:1353–1365
29. Chavhan GB, Babyn PS, Vasanawala SS (2013) Abdominal MR imaging in children: motion compensation, sequence optimization, and protocol organization. Radiographics 33:703–719
30. Courtier J, Rao AG, Anupindi SA (2017) Advanced imaging techniques in pediatric body MRI. Pediatr Radiol 47:522–533
31. Jaimes C, Gee MS (2016) Strategies to minimize sedation in pediatric body magnetic resonance imaging. Pediatr Radiol 46:916–927
32. Arboleda C, Aguirre-Reyes D, García MP et al (2016) Total liver fat quantification using three-dimensional respiratory self-navigated MRI sequence. Magn Reson Med 76:1400–1409
33. Motosugi U, Hernando D, Bannas P et al (2015) Quantification of liver fat with respiratory-gated quantitative chemical shift encoded MRI. J Magn Reson Imaging 42:1241–1248
34. Malamateniou C, Malik SJ, Counsell SJ et al (2013) Motion-compensation techniques in neonatal and fetal MR imaging. AJNR Am J Neuroradiol 34:1124–1136
35. Fujinaga Y, Kitou Y, Ohya A et al (2016) Advantages of radial volumetric breath-hold examination (VIBE) with k-space weighted image contrast reconstruction (KWIC) over Cartesian VIBE in liver imaging of volunteers simulating inadequate or no breath-holding ability. Eur Radiol 26:2790–2797
36. Armstrong T, Dregely I, Stemmer A et al (2018) Free-breathing liver fat quantification using a multiecho 3D stack-of-radial technique. Magn Reson Med 79:370–382
37. Block KT, Chandarana H, Milla S et al (2014) Towards routine clinical use of radial stack-of-stars 3D gradient-echo sequences for reducing motion sensitivity. J Korean Soc Magn Reson Med 18:87–106
38. Armstrong T, Martin T, Stemmer A, et al (2017) Free-breathing fat quantification in the liver using a multiecho 3D stack-of-radial technique: investigation of motion compensation and quantification accuracy. Proc. Int. Soc. Magn. Reson. Med. 25th. p 363
39. Breuer FA, Blaimer M, Heidemann RM et al (2005) Controlled aliasing in parallel imaging results in higher acceleration (CAIPIRINHA) for multi-slice imaging. Magn Reson Med 53:1–8
40. Pineda N, Sharma P, Xu Q et al (2009) Measurement of hepatic lipid: high-speed T2-corrected multiecho acquisition at 1H MR spectroscopy–a rapid and accurate technique. Radiology 252:568–576
41. Ren J, Dimitrov I, Sherry AD et al (2008) Composition of adipose tissue and marrow fat in humans by 1H NMR at 7 Tesla. J Lipid Res 49:2055–2062
42. Hernando D, Kellman P, Haldar JP et al (2010) Robust water/fat separation in the presence of large field inhomogeneities using a graph cut algorithm. Magn Reson Med 63:79–90
43. International Society of Magnetic Resonance in Medicine (2012) ISMRM Fat Water Toolbox. https://www.ismrm.org/workshops/FatWater12/data.htm. Accessed 27 Feb 2012
44. Gleich DF (2009) Models and algorithms for pagerank sensitivity. Dissertation. Stanford University
45. Liu CY, McKenzie CA, Yu H et al (2007) Fat quantification with IDEAL gradient echo imaging: correction of bias from T1 and noise. Magn Reson Med 58:354–364
46. Mann HB, Whitney DR (1947) On a test of whether one of two random variables is stochastically larger than the other. Ann Math Stat 18:50–60
47. Sawilowsky SS (2005) Misconceptions leading to choosing the t test over the Wilcoxon Mann-Whitney test for shift in location parameter. J Mod Appl Stat Methods 4:598–600
48. Bowker AH (1948) A test for symmetry in contingency tables. J Am Stat Assoc 43:572–574
49. Williams S (1996) Pearson's correlation coefficient. N Z Med J 109: 38
50. Lin LI (1989) A concordance correlation coefficient to evaluate reproducibility. Biometrics 45:255–268
51. Bland JM, Altman DG (1999) Measuring agreement in method comparison studies. Stat Methods Med Res 8:135–160
52. Bartlett JW, Frost C (2008) Reliability, repeatability and reproducibility: analysis of measurement errors in continuous variables. Ultrasound Obstet Gynecol 31:466–475
53. Obuchowski NA, Reeves AP, Huang EP et al (2014) Quantitative imaging biomarkers: a review of statistical methods for computer algorithm comparisons. Stat Methods Med Res 24:68–106
54. Rinella ME (2015) Nonalcoholic fatty liver disease: a systematic review. JAMA 313:2263–2273

55. Yu H, McKenzie CA, Shimakawa A et al (2007) Multiecho reconstruction for simultaneous water-fat decomposition and T2* estimation. J Magn Reson Imaging 26:1153–1161
56. Venkatesh SK, Hennedige T, Johnson GB et al (2017) Imaging patterns and focal lesions in fatty liver: a pictorial review. Abdom Radiol 42:1374–1392
57. Lee H, Jun DW, Kang BK et al (2017) Estimating of hepatic fat amount using MRI proton density fat fraction in a real practice setting. Medicine (Baltimore) 96:e7778
58. Hamer OW, Aguirre DA, Casola G et al (2006) Fatty liver: imaging patterns and pitfalls. Radiographics 26:1637–1653
59. Özcan HN, Oğuz B, Haliloğlu M et al (2015) Imaging patterns of fatty liver in pediatric patients. Diagn Interv Radiol 21:355–360
60. Fazeli Dehkordy S, Wolfson T, William Hong C et al (2017) Liver fat reduction following bariatric weight loss surgery is greater in the right lobe of the liver. Proc. Int. Soc. Magn. Reson. Med. 25th. p 123
61. Uecker M, Lai P, Murphy MJ et al (2014) ESPIRiT - an eigenvalue approach to autocalibrating parallel MRI: where SENSE meets GRAPPA. Magn Reson Med 71:990–1001
62. Feng L, Axel L, Chandarana H et al (2016) XD-GRASP: golden-angle radial MRI with reconstruction of extra motion-state dimensions using compressed sensing. Magn Reson Med 75:775–788
63. Horng DE, Hernando D, Reeder SB (2017) Quantification of liver fat in the presence of iron overload. J Magn Reson Imaging 45:428–439
64. Hankins JS, McCarville MB, Loeffler RB et al (2009) R2* magnetic resonance imaging of the liver in patients with iron overload. Blood 113:4853–4855
65. Manco M, Alisi A, Real JMF et al (2011) Early interplay of intrahepatic iron and insulin resistance in children with non-alcoholic fatty liver disease. J Hepatol 55:647–653
66. St Pierre TG, Clark PR, Chua-anusorn W et al (2005) Noninvasive measurement and imaging of liver iron concentrations using proton magnetic resonance. Blood 105:855–861
67. Doyle EK, Toy K, Valdez B et al (2018) Ultra-short echo time images quantify high liver iron. Magn Reson Med 79:1579–1585
68. Krafft AJ, Loeffler RB, Song R et al (2017) Quantitative ultrashort echo time imaging for assessment of massive iron overload at 1.5 and 3 tesla. Magn Reson Med 78:1839–1851
69. Tipirneni-Sajja A, Krafft AJ, McCarville MB et al (2017) Radial ultrashort TE imaging removes the need for breath-holding in hepatic iron overload quantification by R2* MRI. Am J Roentgenol 209:187–194